

Time reversal operator decomposition with focused transmission and robustness to speckle noise: Application to microcalcification detection

Jean-Luc Robert, Michael Burcher, and Claude Cohen-Bacrie
Philips Research USA, 345 Scarborough Road, Briarcliff Manor, New York 10510

Mathias Fink
Laboratoire Ondes et Acoustique, Université Paris 7, ESPCI, 10 rue Vauquelin, 75005 Paris, France

(Received 28 September 2005; revised 3 March 2006; accepted 3 March 2006)

The decomposition of the time reversal operator (DORT) is a detection and focusing technique using an array of transmit-receive transducers. In the absence of noise and under certain conditions, the eigenvectors of the time reversal operator contain the focal laws to focus ideally on well-resolved scatterers even in the presence of strong aberration. This paper describes a new algorithm, FDORT, which uses focused transmission schemes to acquire the operator. It can be performed from medical scanner data. A mathematical derivation of this algorithm is given and it is compared with the conventional algorithm, both theoretically and with numerical experiments. In the presence of strong speckle signals, the DORT method usually fails. The influence of the speckle noise is explained and a solution based on FDORT is presented, that enables detection of targets in complex media. Finally, an algorithm for microcalcification detection is proposed. In-vivo results show the potential of these techniques. © 2006 Acoustical Society of America. [DOI: 10.1121/1.2190163]

PACS number(s): 43.60.Fg, 43.80.Qf, 43.20.Fn [TDM]

Pages: 3848–3859

I. INTRODUCTION

Conventional medical ultrasound systems transmit pulses of sound into the body and map the envelope of returned echoes to form images. The resolution and the signal-to-noise ratio of these images rely on the ability to focus the transmitted pulse in order to maximize the transmitted field around the focal point. In conventional systems, the resolution is limited by diffraction.

In breast ultrasound imaging, as in many medical ultrasound applications, the heterogeneity of the breast degrades the quality of focusing. In particular, the speed of sound in the layer of subcutaneous fat is different from the speed of sound in other tissues. The result of propagation through a medium with variable speed of sound is a distortion of the wavefront and, therefore, a widening of the focal zone. Most of the time, the wavefront is assumed to be only time-delayed, and cross-correlation-based methods are used to find the delays.^{1–3} Those studies show that the distortion can be significant. Then a time delay filter is used to correct for the aberration. The drawback of those methods is the assumption that the propagating medium only induces time-delay distortion. This is only the case if a thin aberrating layer on the transducer surface leads to the distortion. Experimental studies² show that the mean nearest-neighbor correlation coefficient in the breast is 0.8; thus, cross-correlation based methods are not optimal. Moreover, when there are multiple close scatterers, their wavefronts will interfere and a wavefront-following scheme will not lead to an accurate estimation of the aberrator.^{4,5}

Another approach to automatically focus on a well resolved scatterer through heterogeneous media is the time reversal mirror.⁶ However, in a set of well resolved targets, the

time reversal mirror can focus only on the most reflective one.⁷ This led to the development of a detection technique called the DORT (the French acronym for decomposition of the time reversal operator) method. This method is based on the decomposition of the transfer matrix that was introduced to describe the iterative time reversal process.^{8,9} It requires a per-channel transmission and reception scheme (a pulse is sent with one transducer at a time and the echo is recorded on each transducer); this is known as a full data set. In the case of well separated point scatterers and with an acceptable level of noise, the number of significant eigenvalues has been shown⁹ to be equal to the number of scatterers and the corresponding eigenvectors are the frequency Green functions of each scatterer, corresponding to a focusing on the scatterer. The eigenvalue is linked to the target reflectivity. However, DORT use is not limited to point scatterers. Studies¹⁰ have also demonstrated the focusing properties of the time reversal operator's first eigenvector on deterministic extended objects. The advantage of DORT is that its focusing property is independent of any assumption on the aberrator, unlike the usual cross-correlation-based method.

The DORT method has shown great robustness as a detection and focusing method in media with aberration, but other interest arises. The method was not primarily designed to be an imaging method. However, the fact that the method is a frequency-domain process and the analogy between the time reversal matrix and the covariance matrix¹¹ used in passive detection in ocean acoustics or in radar opens the door to array processing methods developed for the latter. There is a large body of literature discussing matched field processing for ocean acoustics¹² and this analogy gives hope that it could be adapted to active array imaging modes like medical ultrasound. Among numerous algorithms, it is worth men-

tioning MUSIC^{11,13,14} (Multiple Signal Classification) which leads to a significant improvement in the resolution: Two wires whose distance was less than one-third of the point spread function, have been separated.¹³ The classical resolution limit is half the point spread function. Image of objects have been reconstructed using the decomposition of the scattering operator, which is the far field limit of the Time Reversal Operator.¹⁵

The DORT method, then, is attractive for use in medical ultrasound imaging. The two main reasons that prevent using the conventional DORT method with medical ultrasound systems are the following: First, most of the ultrasound scanners used for the acquisitions are not very flexible and cannot collect a full data set. They usually transmit a focused beam using several transducers with the appropriate time delays. Second, the importance of speckle signals (sub-resolution scatterers) and the complexity of the scattering medium yield very noisy eigenvectors if the conventional DORT method is used.

Having in scope future medical applications such as aberration correction or array processing, this paper presents a modified DORT method that preserves all the interesting properties of the original method but is designed for data resulting from focused transmits and is efficient in media where speckle is important. We term this method Focused DORT (FDORT). The aim of this paper is not to focus only on medical applications but rather to show that FDORT offer similar results as DORT in theory, simulations, and experiments. As studies on DORT have mainly been conducted on point scatterer distributions,^{8,9} it seems pertinent to use similar setups for comparison purposes and, therefore, most of this paper deals with point scatterers, although they are not prevalent in medical imaging. The interest of a DORT method with focused beams is not limited to medical ultrasound. Experiments have been done in underwater acoustics,¹⁶ and other applications exist in nondestructive evaluation.

Section II addresses the problem of the transmit schemes. It begins with a short review of the principles of the conventional DORT method, with a full data set, mainly to set the formalism, and then establishes the theory of the FDORT method, based on focused transmit acquisitions. More generally the derivations are valid for any shape of the transmit. We address focused pulses as a particular case. Interesting results are summarized in Sec. II C, so that a reader not interested in the mathematical justification can begin at that point. Finally Sec. II D presents simulation results.

Section III discusses the influence of speckle noise on the DORT results. It begins with an explanation of the speckle influence, and proposes a solution based on FDORT to reduce its effect. Experimental results on a medical phantom illustrate the efficiency of the implementation.

Section IV presents an implementation of FDORT restricted to a small area that optimizes the sensitivity of detection of point scatterers in speckle and gives local information on the scattering medium. A method to differentiate point scatterers from extended scatterers or speckle, and thus improve point scatterer detection is proposed and illustrated by an application to *in vivo* microcalcification detection.

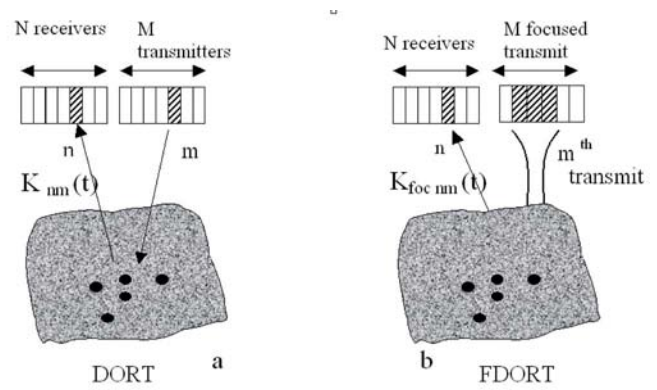


FIG. 1. (a) DORT: Each element of the transmit array is fired individually: Insonification of the medium by element m of the transmit array and reception of the corresponding echo by element n of the receive array gives $k_{nm}(t)$. (b) FDORT: Groups of elements of the transmit array are used to transmit a focused pulse; reception of the echo by element n of the receive array gives $k_{focnm}(t)$.

II. EFFECT OF THE TRANSMIT SCHEME

A. The DORT method: Background theory

1. The transfer matrix and the time reversal operator

The theory of the DORT method has been thoroughly covered in the literature.^{8,9,17} It is introduced here to set the formalism. The method is based on a matrix description of a transmit-receive process performed by an array of transducers,^{8,9} or between two different arrays (an array of M transmitters and an array of N receivers).¹⁷ Most of the DORT experiments are conducted using the same array in transmission and reception, but in order to introduce the modified method in Sec. II B, which uses focused pulses in transmission and per channel reception, we will consider in the following the general case of two different arrays.

If the system (propagation medium and electro-acoustic response) is linear and time-invariant, the process of transmitting and receiving can be described by a collection of filters: Each transmitting element m and each receiving element n are linked by an inter-element impulse response $k_{nm}(t)$, so that:

$$r_n(t) = e_m(t) \otimes k_{nm}(t), \quad (1)$$

where $r_n(t)$ is the signal received on the n th transducer when $e_m(t)$ is transmitted on the m th transducer, as seen in Fig. 1. Thus when the input to element m is a delta impulse, the output of element n is $r_n(t) = k_{nm}(t)$. The Fourier transform yields: $R_n(\omega) = K_{nm}(\omega)$. The repetition of the process for each pair (n, m) of transmitting and receiving elements leads, at a given frequency, to the transfer matrix $\mathbf{K}(\omega)$:

$$\mathbf{K}(\omega) = \begin{bmatrix} K_{11} & K_{12} & \cdots & K_{1M} \\ K_{21} & K_{22} & & \\ \vdots & & \ddots & \\ K_{N1} & & & K_{NM} \end{bmatrix}$$

The matrix K describes the propagation between the transmit and the receive arrays and is therefore dependent on the scattering medium. If a signal $\mathbf{E}(\omega) = [E_1(\omega), E_2(\omega), \dots, E_M(\omega)]^T$, where $E_m(\omega)$ is the input of

element m , at the frequency ω and T is the transpose (that transforms a $1 \times M$ row vectors into a $M \times 1$ column vector) is transmitted into the medium, the received echo is given by the following matrix formulation:

$$\mathbf{R}(\omega) = \mathbf{K}(\omega)\mathbf{E}(\omega), \quad (2)$$

where $\mathbf{R}(\omega)=[R_1(\omega), R_2(\omega), \dots, R_N(\omega)]^T$, $R_n(\omega)$ being the signal received by the n th element of the receive array. $\mathbf{E}(\omega)$ and $\mathbf{R}(\omega)$ are vectors expressed in the transmit and receive basis, respectively, formed by the elements of the arrays. Reference to the frequency ω is omitted in the following. To perform time reversal, the receive (R_x) array has to transmit back the time reversed signal (corresponding to a phase conjugation in the frequency domain) $\overline{\mathbf{K}\mathbf{E}}$ and the transmit (T_x) array has to receive it (during the time reversal the role of both arrays are exchanged). Because of the reciprocity theorem, the propagation from the receive to the transmit array is given by \mathbf{K}^T . The signal received by the T_x array at the end of the *time reversal cycle* is then $\mathbf{K}^T\overline{\mathbf{K}\mathbf{E}}$, which is simply the conjugate of $(\mathbf{K}^H\mathbf{K})\mathbf{E}$, where \mathbf{H} stands for the Hermitian, or conjugate, transpose (transpose followed by conjugation), and $\mathbf{T}_{T_x} = \mathbf{K}^H\mathbf{K}$ is defined as the time reversal operator expressed in the T_x array (T_x basis). We can similarly define the time reversal operator from the R_x array point of view: $\mathbf{T}_{R_x} = \mathbf{K}\mathbf{K}^H$.

For all the results recalled here, there is no need for \mathbf{K} to be either symmetric or square (which is obviously not the case if N is not equal to M) as it was in the earliest papers.⁸ Then in general $\mathbf{K}^H\mathbf{K}$ and $\mathbf{K}\mathbf{K}^H$ are different, but both have the same rank, equal to the rank of \mathbf{K} .

As $(\mathbf{K}^H\mathbf{K})^H = \mathbf{K}^H\mathbf{K}$ the time reversal operator is Hermitian positive in an orthogonal basis and thus can be diagonalized. Moreover, the eigenvalues are real and positive, and the eigenvectors are orthogonal.

The DORT method is based on the diagonalization of this time reversal operator. Section II A 2 describes the information given by the method in a simple case.

Practically, the diagonalization of the time reversal operator is not used. Indeed, it is mathematically equivalent to the singular value decomposition (SVD) of \mathbf{K} :

$$\mathbf{K} = \mathbf{U}\mathbf{S}\mathbf{V}^H, \quad (3)$$

where \mathbf{S} is a $N \times M$ diagonal matrix completed by lines of zeros, containing the singular values of \mathbf{K} ; \mathbf{U} is a $N \times N$ unitary matrix whose columns are the eigenvectors of $\mathbf{K}\mathbf{K}^H$ (the time reversal operator expressed in the receive basis); and \mathbf{V} is the $M \times M$ matrix whose columns are the eigenvectors of $\mathbf{K}^H\mathbf{K}$.

2. Case of isotropic, pointlike scatterers, and single scattering

a. Expression of the transfer matrix. In the case of isotropic point scatterers and under the Born approximation, the eigenvectors and eigenvalues of the time reversal operator can be theoretically calculated. For clarity, the number of point scatterers is assumed to be two. Let \mathbf{P} and \mathbf{Q} be the scatterers' positions. We denote by $\mathbf{H}_{R_x}(\mathbf{P})$ and $\mathbf{H}_{T_x}(\mathbf{P})$ the monochromatic Green functions of \mathbf{P} expressed in the R_x and

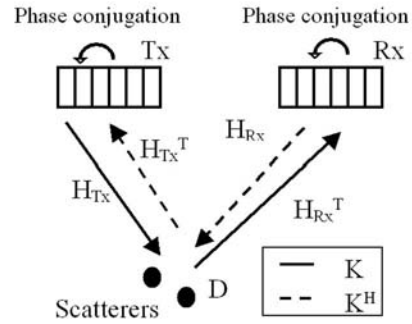


FIG. 2. The time reversal process can be seen as a full cycle between 3 actors: The T_x array, the R_x array and the scatterers. Propagation between the actors is described by \mathbf{H}_{T_x} and \mathbf{H}_{R_x} . Reflection from the scatterers is equivalent to a multiplication by \mathbf{D} , and the backpropagation by the arrays is equivalent to a phase conjugation, included in the hermitian transpose \mathbf{H} . \mathbf{K} describes the one-way propagation between T_x and R_x , represented by the solid line. The time reversal operator can be expressed mathematically from the point of view of any of these 3 actors. Then one has to start from the desired actor and make a full cycle.

T_x bases, respectively. For example, $\mathbf{H}_{T_x}(\mathbf{P})$ is a $1 \times M$ vector and $H_{T_x}(\mathbf{P})_m$ describes the propagation between the i th element and \mathbf{P} . Let $D(\mathbf{P})$ and $D(\mathbf{Q})$ be the reflectivity of each scatterer. We also assume the absence of noise and we omit the acousto-electrical responses of the transducers, as they have no influence on the results.

A transmit-receive process can be divided into three stages, as seen in Fig. 2: Propagation from the T_x array to the scatterers, reflection on the scatterers, and finally propagation to the R_x array. The transmit-receive process between T_x element m and R_x element n is then: $\mathbf{K}_{nm} = H_{T_x}(\mathbf{P})_m D(\mathbf{P}) H_{R_x}(\mathbf{P})_n + H_{T_x}(\mathbf{Q})_m D(\mathbf{Q}) H_{R_x}(\mathbf{Q})_n$ and finally, one can write the transfer matrix as the product of 3 terms:⁸

$$\mathbf{K} = (\mathbf{H}_{R_x})^T \mathbf{D} \mathbf{H}_{T_x}, \quad (4)$$

where

$$\mathbf{H}_{R_x} = \begin{pmatrix} H_{R_x}(\mathbf{P})_1 & H_{R_x}(\mathbf{P})_2 & \cdots & H_{R_x}(\mathbf{P})_N \\ H_{R_x}(\mathbf{Q})_1 & H_{R_x}(\mathbf{Q})_2 & \cdots & H_{R_x}(\mathbf{Q})_N \end{pmatrix},$$

and

$$\mathbf{D} = \begin{pmatrix} D(\mathbf{P}) & 0 \\ 0 & D(\mathbf{Q}) \end{pmatrix}.$$

\mathbf{H}_{T_x} has the same structure as \mathbf{H}_{R_x} ; its rows are the Green functions expressed in the T_x array. It follows from Eq. (4) that the rank of \mathbf{K} is equal to the number of scatterers.

b. Time reversal operator from the scatterers' point of view. In the receive basis, the time reversal operator becomes:

$$\mathbf{K}\mathbf{K}^H = (\mathbf{H}_{R_x})^T \mathbf{D} \mathbf{H}_{T_x} \mathbf{H}_{T_x}^H \overline{\mathbf{D}} \mathbf{H}_{R_x}. \quad (5)$$

Although experimentally we only have access to the time reversal operator expressed from the point of view of one of the arrays, in order to understand the properties of its eigenvectors, it is more convenient to express it from the point of view of the scatterers, in other words in the scatterers' basis. As depicted in Fig. 2, the time reversal process can be seen as a cycle. From the scatterers' point of view, the cycle begins at the scatterers location and is seen as follows: The scatterers emit an echo toward the R_x array, which back-

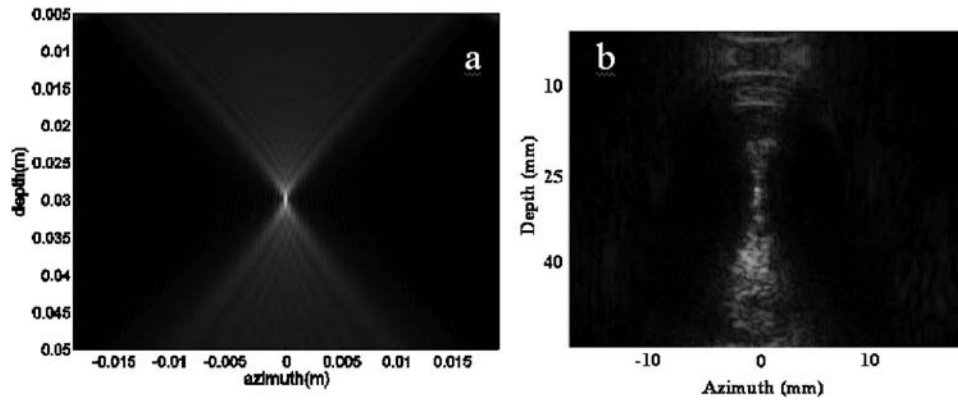


FIG. 3. (a) Magnitude of the field resulting from focusing on a scatterer (“the target”) located at depth $z=30$ mm. The shadow of the transducer, in gray, is the coupling area. Any scatterer located in that area is coupled with the first one: The eigenvectors of the time reversal operator are then linear combination of the scatterers’ Green functions. If the second scatterer is located outside of the shadow in the black area, the scatterers are well resolved and the Green functions are separated, each corresponding to one eigenvector. (b) Map of scatterers coupled to a given target ($x=0$, $z=25$ mm) in a medical image. The backscatter signal has been projected onto the target Green function before the beamforming and then only the scatterers whose Green functions are not orthogonal to the target’s are imaged with an intensity proportional to the coupling.

propagates the echo toward the scatterers. The signal is reflected by the scatterers, received by the Tx array and back-propagated one more time toward the scatterers. Let \mathbf{T}_{scat} be the time reversal operator in the scatterer basis; as there are two scatterers, \mathbf{T}_{scat} is a 2×2 matrix and $\mathbf{T}_{\text{scat},ij}$ is the signal received by scatterer i after a full time reversal process when the initial echo was sent by scatterer j . \mathbf{T}_{scat} is expressed as

$$\mathbf{T}_{\text{scat}} = \mathbf{D} \mathbf{H}_{\text{Tx}} \mathbf{H}_{\text{Tx}}^H \overline{\mathbf{D}} \overline{\mathbf{H}}_{\text{Rx}} \mathbf{H}_{\text{Rx}}^T. \quad (6)$$

Furthermore,

$$\overline{\mathbf{H}}_{\text{Rx}} \mathbf{H}_{\text{Rx}}^T = \begin{pmatrix} \|\mathbf{H}_{\text{Rx}}(\mathbf{P})\|^2 & \langle \mathbf{H}_{\text{Rx}}(\mathbf{Q}) | \mathbf{H}_{\text{Rx}}(\mathbf{P}) \rangle \\ \langle \mathbf{H}_{\text{Rx}}(\mathbf{P}) | \mathbf{H}_{\text{Rx}}(\mathbf{Q}) \rangle & \|\mathbf{H}_{\text{Rx}}(\mathbf{Q})\|^2 \end{pmatrix}. \quad (7)$$

And a similar expression holds for $\mathbf{H}_{\text{Tx}} \mathbf{H}_{\text{Tx}}^H$. Because \mathbf{D} is already diagonal, a condition for the expression of Eq. (6) to be diagonal is:

$$\langle \mathbf{H}_{\text{Rx}}(\mathbf{P}) | \mathbf{H}_{\text{Rx}}(\mathbf{Q}) \rangle = 0, \quad (8)$$

which means that $\overline{\mathbf{H}}_{\text{Rx}} \mathbf{H}_{\text{Rx}}^T$ is diagonal, and

$$\langle \mathbf{H}_{\text{Tx}}(\mathbf{P}) | \mathbf{H}_{\text{Tx}}(\mathbf{Q}) \rangle = 0, \quad (9)$$

which means that $\mathbf{H}_{\text{Tx}} \mathbf{H}_{\text{Tx}}^H$ is diagonal. In other words, the Green functions of the scatterers are orthogonal in both the transmit [Eq. (9)] and the receive [Eq. (8)] bases.

c. Physical interpretation. There is a physical interpretation of the scalar products from Eqs. (8) and (9). Using time-reversal arguments, transmitting $\overline{\mathbf{H}}_{\text{Rx}}(\mathbf{Q})$ with the receive array results in focusing on the point \mathbf{Q} . The field received at the point \mathbf{P} when transmitting such a signal is expressed as

$$\sum_{m=1}^N \overline{\mathbf{H}}_{\text{Rx}}(\mathbf{Q})_m \mathbf{H}_{\text{Rx}}(\mathbf{P})_m = \langle \mathbf{H}_{\text{Rx}}(\mathbf{P}) | \mathbf{H}_{\text{Rx}}(\mathbf{Q}) \rangle. \quad (10)$$

Thus the scalar product is equal to zero if it is possible to focus on one scatterer without sending energy to the other one, as illustrated in Fig. 3. The scatterers are then said to be well resolved or well separated.

d. Eigenvectors. The conditions of Eqs. (8) and (9) are satisfied if the scatterers are well resolved from the point of view of both arrays. In this case, Eq. (8) shows that the time reversal operator is diagonal in the scatterers’ basis. The two

eigenvectors of the time reversal operator expressed in the Rx basis [Eq. (5)] associated with nonzero eigenvalues are then the scatterers’ Green functions, $\mathbf{H}_{\text{Rx}}(\mathbf{P})$ and $\mathbf{H}_{\text{Rx}}(\mathbf{Q})$ expressed in the Rx array. Identically, eigenvectors of the time reversal operator expressed in the Tx basis are the Green function in the Tx array. The SVD of K [Eq. (3)] gives the eigenvectors in both the Rx and Tx array. Moreover, the eigenvalue corresponding to the scatterer \mathbf{P} is

$$\lambda = \|\mathbf{H}_{\text{Tx}}(\mathbf{P})\|^2 \|\mathbf{H}_{\text{Rx}}(\mathbf{P})\|^2 D(\mathbf{P})^2.$$

If the targets are not well resolved, there is a coupling between them through the nonzero diagonal terms of Eq. (7) and the eigenvectors are expressed as a linear combination of the Green functions.⁹ The transmission of such an eigenvector does not lead to point focusing but DORT still provides useful information in this case. In particular, matched field methods like MUSIC can still be used.¹³

The assumption of isotropic scattering, used for the calculations, is true only for a point-like discontinuity in compressibility. Dipole scattering that accounts for discontinuities in density can be incorporated with additional complexity.¹⁸

B. The DORT method with focused pulse acquisitions (FDORT): Theory

1. The generalized transfer matrix

The transfer matrix for DORT is built on a full data set. In medical ultrasound, insonifications are usually obtained using a different process. Many elements of the array are fired with appropriate time delays (and apodization) to focus the energy at a specific location. The reflected signal, which largely originates from this region, is then recorded on the elements of the same array. The next pulse is sent using a different delay law, to focus the energy at a nearby location, and so on. At a given frequency, each transmitted pulse is expressed as a complex vector in the array basis. Assuming that M different focused pulses are transmitted during the acquisition, using a N -element array, let \mathbf{B}_m be the $N \times 1$ vector describing the m th transmitted pulse focusing at a position \mathbf{X}_m . The coefficients of \mathbf{B}_m are the amplitude and phase

of the signal transmitted by each element of the array and are typically given by $B_{mn} = A_{mn} e^{j(\omega d_{mn}/c)}$ where d_{mn} is the distance between the array element n and the focal point \mathbf{X}_m , and A_{mn} is an apodization term.

We define \mathbf{B} as the $M \times N$ matrix whose m th row is the vector \mathbf{B}_m .

Building a second transfer matrix using the signals received on each element with focused transmit pulses gives the generalized transfer matrix \mathbf{K}_{foc} . $(K_{\text{foc}})_{mn}$ is the signal received on element n for the m th focused transmit, as seen in Fig. 1. \mathbf{K}_{foc} can be expressed in terms of \mathbf{K} , the *true* transfer matrix described earlier:

$$\mathbf{K}_{\text{foc}} = \mathbf{K} \mathbf{B}^T. \quad (11)$$

If one chooses a family of vectors forming a basis, then \mathbf{B} is known and invertible and it is possible to get back to the transfer matrix \mathbf{K} using $\mathbf{K} = \mathbf{K}_{\text{foc}} (\mathbf{B}^T)^{-1}$. However, in the general case, as in our experiments, the \mathbf{B}_m are not necessarily linearly independent, therefore, they do not form a basis. In the following \mathbf{B} is considered to be noninvertible and unknown.

2. Case of isotropic, pointlike scatterers and single scattering

Substituting Eq. (4) into Eq. (11), it is still possible to express \mathbf{K}_{foc} as

$$\mathbf{K}_{\text{foc}} = (\mathbf{H}_{\text{Rx}})^T \mathbf{D} \mathbf{H}_{\text{Rx}} \mathbf{B}^T. \quad (12)$$

It is worth noting that the same array is used in transmission and in reception in this section. \mathbf{H}_{Rx} refers here to the propagation matrix between this one array and the scatterers. The rows of \mathbf{H}_{Rx} are then the scatterers's Green function expressed in the array basis.

Defining \mathbf{H}_{Tx} to be

$$\mathbf{H}_{\text{Tx}} = \mathbf{H}_{\text{Rx}} \mathbf{B}^T, \quad (13)$$

\mathbf{K}_{foc} can be expressed as

$$\mathbf{K}_{\text{foc}} = (\mathbf{H}_{\text{Rx}})^T \mathbf{D} \mathbf{H}_{\text{Tx}},$$

as in the case of two different arrays introduced in Sec. I A 2. Therefore, from a mathematical standpoint, the process can be described like a classical DORT method between two different arrays. The receive array is a physical array, but the transmit array is here purely virtual. Coordinates of a vector in this array are given by the projection of the vector onto each \mathbf{B}_i . In the case of the focused beams, everything happens as if there were virtual transmit elements located at the foci of the beams and having a certain directivity angle.^{19,20} The following derivations are not restricted to focused transmits.

This analogy yields the possibility to use the results of Sec. II A 2. A *pseudo* time reversal operator can then be built in the receive basis by choosing $\mathbf{T}_{\text{Rx}} = \mathbf{K}_{\text{foc}} (\mathbf{K}_{\text{foc}})^H$. A condition for this *pseudo* time reversal operator to be diagonal in the scatterers' basis is again given by Eqs. (8) and (9). The physical interpretation of Eq. (8) is that the scatterers must be well-resolved by the array.

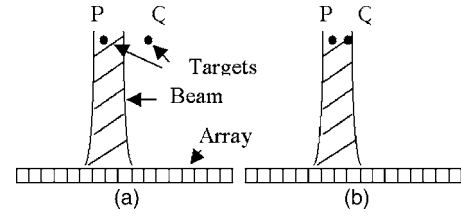


FIG. 4. Coupling condition with focused transmit. (a) The distance between the scatterers is greater than the width of the PSF; each beam insonifies only one scatterer, and they are not coupled. (b) the scatterers have a separation smaller than the point spread function; consequently, a beam may insonify both scatterers. In this case they are coupled.

Interpretation of Eq. (9) is not so straightforward as \mathbf{H}_{Tx} does not correspond to a real array: One has to notice that, in the case of two scatterers \mathbf{P} and \mathbf{Q}

$$\begin{aligned} \mathbf{H}_{\text{Tx}} &= \begin{pmatrix} \langle \mathbf{B}_1 | \mathbf{H}_{\text{Rx}}(\mathbf{Q}) \rangle & \langle \mathbf{B}_2 | \mathbf{H}_{\text{Rx}}(\mathbf{Q}) \rangle & \cdots & \langle \mathbf{B}_M | \mathbf{H}_{\text{Rx}}(\mathbf{Q}) \rangle \\ \langle \mathbf{B}_1 | \mathbf{H}_{\text{Rx}}(\mathbf{P}) \rangle & \langle \mathbf{B}_2 | \mathbf{H}_{\text{Rx}}(\mathbf{P}) \rangle & \cdots & \langle \mathbf{B}_M | \mathbf{H}_{\text{Rx}}(\mathbf{P}) \rangle \end{pmatrix}. \end{aligned} \quad (14)$$

Following Eq. (11)

$$\mathbf{H}_{\text{Tx}} = \begin{pmatrix} F_1(\mathbf{Q}) & F_2(\mathbf{Q}) & \cdots & F_M(\mathbf{Q}) \\ F_1(\mathbf{P}) & F_2(\mathbf{P}) & \cdots & F_M(\mathbf{P}) \end{pmatrix}, \quad (15)$$

where $F_m(\mathbf{Q})$ is the field obtained at position \mathbf{Q} when the m th focused pulse is transmitted. Now the condition (9) is

$$\sum_{m=1}^M F_m(\mathbf{Q}) \bar{F}_m(\mathbf{P}) = 0. \quad (16)$$

This condition is valid for any shape of the transmit beams and means that the series $F_m(\mathbf{Q})$ and $F_m(\mathbf{P})$ are uncorrelated. In other words, the scatterers have to be insonified in an uncorrelated way. For focused beams and supposing that the scatterers are at the same depth and separated by a lateral distance Δx , Eq. (16) can be rewritten as

$$C_0 F(x - \Delta x, z) \otimes_x F(-x, z) = C_0 R_{FF}(\Delta x) = 0, \quad (17)$$

with $F(x, z)$ being the beam pattern at the scatterers' depth and R_{FF} its autocorrelation function, as shown in the Appendix. If no apodization is used (rectangular transmit aperture), this simplifies to

$$F(\Delta x, z = f) = 0, \quad (18)$$

where f is the focal depth. The two scatterers have to be resolved by the transmit focused beam, or in other words Δx must be greater than the resolution of the beam. For two scatterers located in the focal plane of the array, this can be understood easily; indeed, each focused pulse insonifies only a limited part of the medium. In the focal plane, this area is the point spread function. The sum of Eq. (16) can only be nonzero if at least one of the products is nonzero; In other words, at least one pulse has to insonify both location \mathbf{P} and \mathbf{Q} as depicted in Fig. 4. If the targets are located so that no pulse insonifies more than one target, then the condition of Eq. (16) is realized. It is important to note that the coupling condition is independent of the focal depth of the array and

the presence of aberration, as demonstrated in the Appendix. FDORT, like DORT, is then robust in the presence of an aberrator. The derivation in the Appendix makes apparent a condition on the beam spacing: It must be smaller than the beam resolution, which is a classic condition in imaging and can be related to the sampling theorem.

Again, if both conditions of Eqs. (8) and (16) are realized, the *pseudo* time reversal operator is diagonal in the scatterers basis, and we deduce that the eigenvectors of the time reversal operator expressed in the receive basis are the Green functions of the point scatterers as seen by the array. Note that the eigenvectors in the transmit basis (also provided by the SVD of \mathbf{K}_{foc}) show how much each scatterer is insonified by each focused beam. The eigenvalue associated with the scatterer P is then given by Eqs. (6), (7), and (13)

$$\lambda(\mathbf{P}) = \|\mathbf{H}_{\text{Rx}}(\mathbf{P})\mathbf{B}^T\|^2 \|\mathbf{H}_{\text{Rx}}(\mathbf{P})\|^2 D(\mathbf{P})^2. \quad (19)$$

C. Main results and comparison between DORT and FDORT

The first step of the FDORT method is to **build a generalized transfer matrix**. At a given frequency, the coefficients of this matrix are the Fourier coefficients of the receive signals on each of the N array elements for each of the M transmit focused pulses. Each column of the matrix corresponds to one transmit focused pulse, and each row corresponds to the signal received by one element. Then, a **singular value decomposition of the transfer matrix is computed** as shown in Eq. (3). If the point scatterers are well separated so that there is no coupling between them, the number of non-zero singular values in S gives the number of point scatterers in the medium and their reflectivities. The corresponding singular vectors in U are the Green functions of each scatterer as seen by the array. Backpropagation of these singular vectors in the medium leads to a focusing at the position of the scatterers, even in the presence of aberration.

This implementation and the results of FDORT are very similar to the DORT method. We now want to compare DORT, using the same array of N elements in both transmit and receive as it is usually implemented, and FDORT, using the same array of N elements. Usually, in a scanner, only a fraction of the total aperture is used for each transmission. Here, each focused pulse for FDORT is assumed to be transmitted with half the aperture ($N/2$ elements), which is the case in the simulations. The main difference between DORT and FDORT is the ability to separate two scatterers, so that each eigenvector is the Green function of one scatterer. This is here referred to as the resolution. For **DORT, the ability to separate two scatterers depends only on the total aperture**. For **FDORT, the dependence is on both the Rx process [Eq. (8)] depending on the whole aperture, and the Tx process [Eq. (18)], determined here by the half aperture**. This is in fact the same resolution condition that one has in conventional imaging. The **resolution is then slightly lower** with FDORT. An important result, *a priori* not obvious, is that if all the elements were used for each transmit with FDORT, FDORT would yield results comparable to DORT (using same array in Rx and Tx). Results are summarized in Table I.

TABLE I. Comparison of DORT and FDORT.

	DORT	FDORT
Data	Full data set	Focused transmit pulses
Separation of scatterers	Given by the total aperture: N elements	Limited by the transmit aperture: $N/2$ elements here
Singular values	1 nonzero eigenvalue per scatterer, depend on the reflectivity	1 nonzero eigenvalue per scatterer, depend on the reflectivity
Singular vectors in U (eigenvector of the time reversal operator in thereceive basis)	Green function of each scatterer as seen by the array	Green function of each scatterer as seen by the array
Singular vectors in V (eigenvector of the time reversal operator in the transmit basis)	Green function of each scatterer as seen by the array	No information on the Green function, but shows the signal transmitted by each focused pulse on the scatterer

However, one of the **main advantage of FDORT** is the **possibility to use focused transmit and also to implement the algorithm** presented in Secs. III and IV.

D. Simulations

A Philips one-dimensional (1D) linear array at 7.3 MHz center frequency is simulated using Field2 [J. A. Jensen, DTU] along with two point scatterers separated by 2 mm, both in the focal plane of the array. A phase-screen aberrator with parameters rms (root mean square) = 30 nm and FWHM (full width half max) = 4 mm is placed at the array surface. $M=100$ focused transmissions separated by 0.1 mm are used. For each transmission, the backscatter signal is recorded on each of the elements. A Fast Fourier Transform of the $N \times M$ signals is taken to build the generalized transfer matrix at several frequencies. A singular value decomposition algorithm is used to compute eigenvalues and eigenvectors of the time reversal operator. Results are shown in Fig. 5. Two significant eigenvalues are observed. The corresponding eigenvectors are found to focus very accurately on each of the scatterers through the aberrator.

To compare the coupling condition of both algorithms, another simulation is ran where the distance between the 2 scatterers is reduced progressively from 1 mm to 0. The eigenvalues, which are function of the coupling are computed for both FDORT and DORT and displayed in Fig. 6. The same experiment is repeated with an aberrator and for scatterers out of the focal plan to show that this does not influence FDORT. As it is known⁹ that coupling is responsible for an increase of the first eigenvalue and a decrease of the second one, the evolution of eigenvalues show the appearance

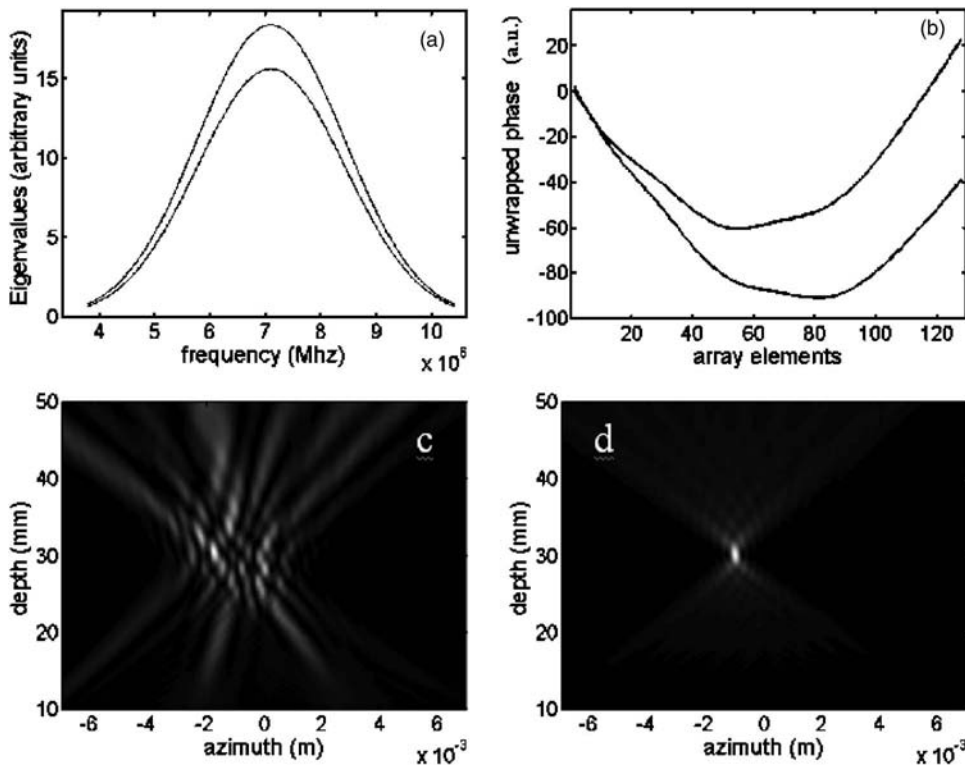


FIG. 5. Results of FDORT performed on simulated data with 2 scatterers and an aberrator. (a) Eigenvalues as a function of frequency: Two eigenvalues have a significant magnitude, corresponding to the two scatterers. (b) Phase of the corresponding eigenvectors at the central frequency. It is proportional to the focal delay law to focus on each of the targets. In particular, it contains the delay law introduced by the aberration. (c) Intensity of the field transmitted in the medium when a simple geometric delay law is used to focus on one of the targets. The aberration results in poor focusing. (d) Intensity of the transmitted field when one of the eigenvectors is used to focus on the target.

and increase of coupling when the distance decreases.

III. ADAPTATION OF FDORT FOR A NOISY ENVIRONMENT

The DORT and FDORT methods are able to detect and focus on well separated point scatterers, like wires (which can be considered point-like in the 2D geometry of the experiments), in water, even in the presence of a strong

aberrator.⁹ In medical applications, however, the scatterers are embedded in tissue that generates a speckle signal. The FDORT process was performed on a tissue-mimicking phantom with wire-targets, represented in Fig. 7. Eigenvalues and numerical backpropagation of the second eigenvectors are shown in Fig. 8 (bottom). Due to speckle, the eigenvectors become too noisy and FDORT, like DORT, fails: Focusing on the wires' locations is very poor. The next step, then, is to

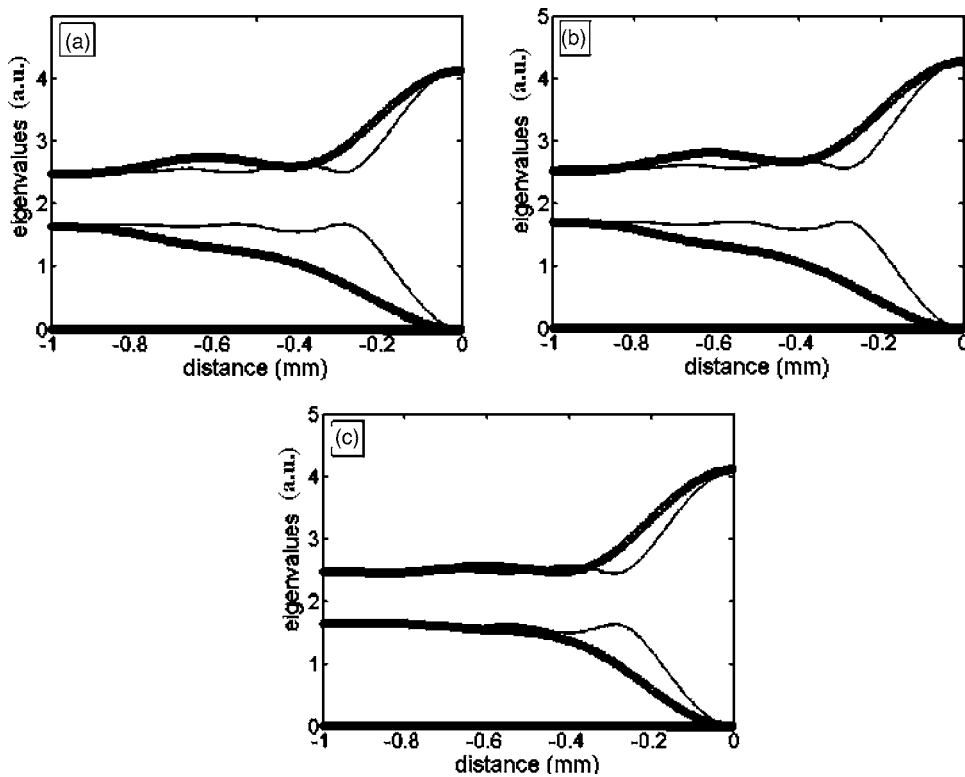


FIG. 6. Eigenvalues of DORT (thin line) and FDORT (thick line) vs distance for two scatterers located at the same depth (a) in the focal plane of the array ($f=20$ mm), (b) in the focal plane but in presence of aberration, and (c) out of the focal plane, at depth 30 mm. When the scatterers are too close, coupling occur and results in a separation of the eigenvalues. The importance of coupling depends on how well the scatterers are resolved by both transmit and receive array. It occurs over a larger range with FDORT because only half the aperture is used in transmission. FDORT's ability to separate two targets response is not degraded by aberration or for scatterers out of the focal plane. DORT and FDORT eigenvalues have been normalized to appear on the same scale.

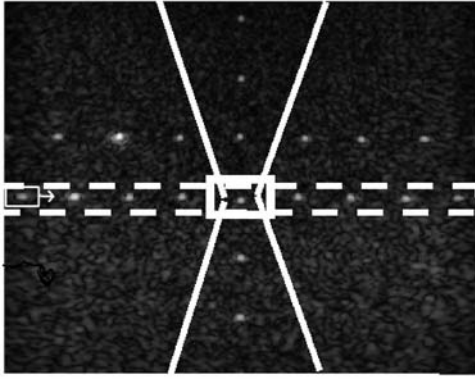


FIG. 7. Tissue-mimicking phantom used for the experiments. The zone of coupling for one scatterer is indicated by the white conical shape. Scatterers inside this area are coupled with the scatterer. The box drawn with dashed lines indicates the area used in Sec. III, obtained by time gating the signals. This reduces the influence of the coupled scatterers. The box in solid lines indicates the area used for Local FDORT in Sec. IV.

adapt the method to work in such an environment. For simplicity, the case of point scatterers in a speckle-generating medium will be considered first. The aim is to be able to detect the point scatterers and obtain a good focusing on each of them, despite the strong speckle signal. A good focus is indeed required for target detection, or if one's aim is to image a medium, for aberration correction.

A. Influence of noise on eigenvectors and eigenvalues

In this part is considered only the problem of acoustic noise, in particular speckle noise. Indeed, the influence of the electronic noise is already known. It is spatially uncorrelated and thus it can be shown¹³ that the time reversal operator at a given frequency can be approximated by

where $(\mathbf{H}_{\text{Rx}})^T \mathbf{D} \mathbf{H}_{\text{Tx}} (\mathbf{H}_{\text{Tx}})^H \mathbf{D} \mathbf{H}_{\text{Rx}}$ is the time reversal operator in the absence of noise [Eq. (5)], M is the number of transmit pulses, σ^2 is the noise power, and \mathbf{I} is the identity matrix. The eigenvectors of the time reversal operator remain unchanged and the eigenvalues are uniformly increased by $M\sigma^2$. Thus, a small amount of electronic noise has then no influence on the DORT or FDORT process.

The influence of acoustic noise is more complicated. Signals from scatterers other than the ones we want to detect (here the wires in the phantom) are considered as noise. In that case these are sub-resolution scatterers generating speckle signal. Two cases can be distinguished:

a. Ideally separated scatterers. These are not coupled with the targets; they are located outside the coupling area for each target, as depicted on Fig. 3. They give rise to new nonzero eigenvalues, but do not affect the eigenvectors corresponding to the targets that still enable perfect focusing. The focusing properties are preserved, but as there are more nonzero eigenvalues, it is more difficult to determine which eigenvectors correspond to the targets. The difference with sensor noise is that the eigenvalues are not uniformly increased: eigenvalues corresponding to noise can now have higher values than the ones from targets.

b. Nonideally separated scatterers. They are coupled with the targets. There are more nonzero eigenvalues, as in the previous case, but here the eigenvectors are affected: They are no longer equal to the Green functions of individual targets, but are linear combinations of the targets' Green functions and Green functions from noise scatterers coupled with the targets. The resulting eigenvectors can be very complex in the presence of speckle signals, as hundreds of sub-resolution scatterers are coupled with the target. Figure 3(b) represents, in a clinical image, all the scatterers coupled with

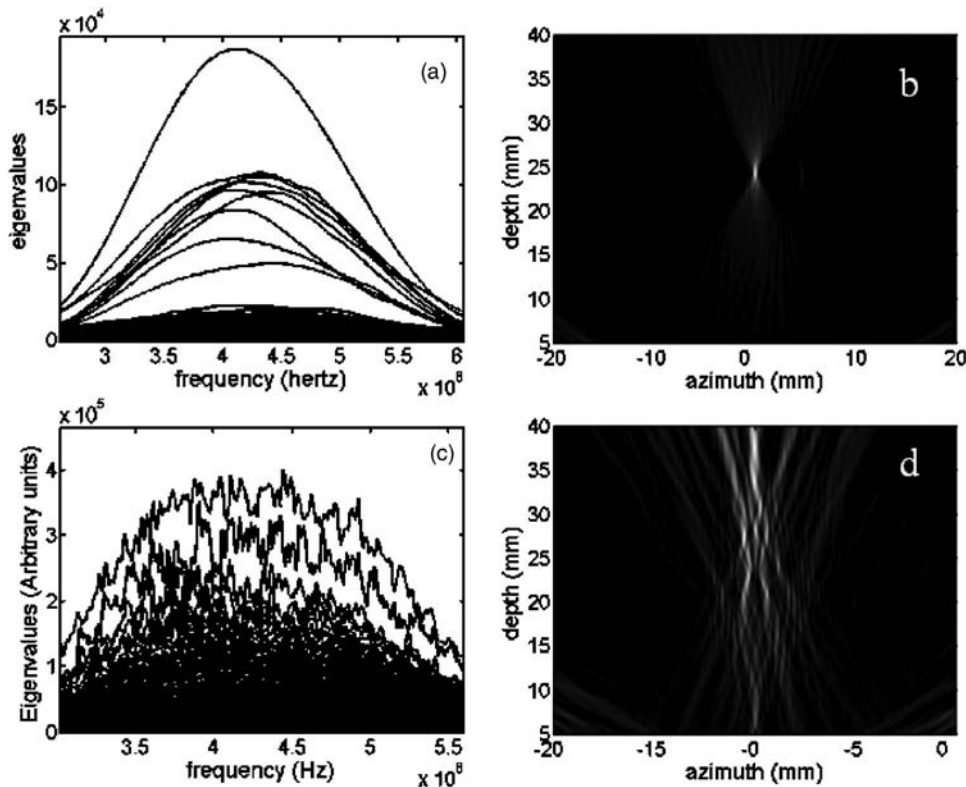


FIG. 8. The FDORT method has been performed on a tissue-mimicking phantom with wires. Top: Eigenvalues vs frequency (a) and intensity (b) of the field resulting from the backpropagation of the second eigenvector, when FDORT is restricted to a slice around depth $z=25$ mm where 9 wires are located, using time gating. Nine significant eigenvalues are observed and the eigenvectors focus accurately on the wires. Bottom: The same experiment but without time gating. The focusing property of the eigenvectors is dramatically reduced, because of the coupling with the speckle.

the target, located at a depth of 25 mm. The focusing properties are in this case dramatically degraded, as seen in Fig. 8.

B. A solution: FDORT with time gating

1. Principle

We are here interested to reduce the effect of the last kind of noise, which has the worst influence. The noise comes from the set of scatterers coupled with the target, contained in a conical shape centered on the target. Laterally, in the target plane, the zone of coupling is narrow. It was shown in Sec. II. this is determined by the classic point spread lateral extension. This limitation is due to the finite size of the array and affect usual beamforming imaging. Axially the coupled zone is much more extended. This limit is not present in classical beamforming. It is due to the fact that the temporal resolution is not exploited by DORT or FDORT because of their only monochromatic nature. An important amount of information is then lost. To solve this difficulty, impulsive, and monochromatic approaches have to mixed. At any given time τ , an incident ultrasound beam illuminates only a volumetric distribution of scatterers, called the isochronous volume.^{21,22} Now, selecting within the echographic signal an analysis time window $[\tau, \tau + \Delta\tau]$ is equivalent to selecting only echoes from scatterers located in a well-defined volume whose lateral extension is equal to the lateral extension of the beam, and whose axial extension Δz is related to $\Delta\tau$. If we repeat this process for every beam, the union of all the volumes gives a slice of the medium of width Δz , represented in Fig. 7. From the point of view of FDORT, using time windows is similar to having an empty medium outside this slice. Therefore, there is no coupling with scatterers outside of the slice. Thanks to time gating, the zone of coupling narrows axially and tends to the limit set by the temporal resolution; targets from different depths can then be fully decoupled if advantage is taken from the impulsive approach.

Such a process is possible only with focused pulse transmission. If a single element transmission is used, as in the classical DORT method, the whole medium is insonified and it is no longer feasible to select signals from a given depth.

2. Experiments

Experiments are carried out on the medical phantom represented in Fig. 7, using a Philips HDI-5000 and a 1D linear array at 4.3 MHz center frequency.

For each transmission the signals on all N received elements are recorded. The signals are gated in time, keeping only the signal from $z - 0.5\Delta z$ to $z + 0.5\Delta z$. The window width is chosen to be slightly longer than the pulse width. For the m th transmission pulse, gating in depth is achieved using the geometrical focal law focusing along the beam m at depth z .

Figure 8 (top) shows the eigenvalue spectrum and the numerical backpropagation of the first eigenvectors obtained using the FDORT method in the medical phantom at the depth of 9 wires. It demonstrates a great improvement in the focusing ability of the first eigenvectors, compared to the

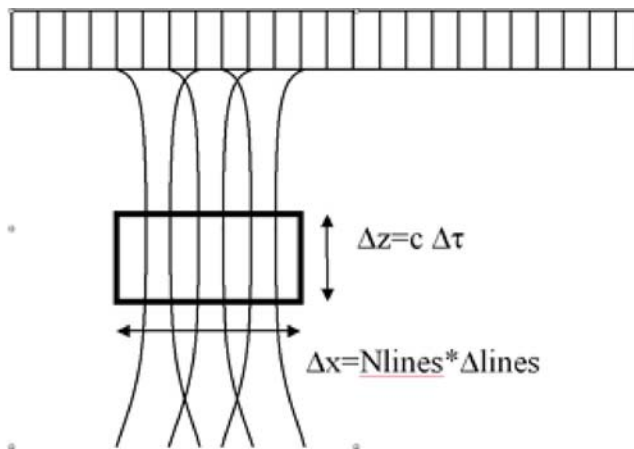


FIG. 9. Shows how FDORT can be restricted to a small area (the black window depicted): Windowing in depth (Δz) is achieved by time gating ($\Delta\tau$) of the signals and windowing in azimuth (Δx) is achieved by the number (N_{lines}) of consecutive lines used: On the picture, three lines are used. $\Delta lines$ is the distance between two consecutive lines (the beam spacing).

results in Fig. 8 (bottom). To obtain the focal law of each wire, one needs to repeat the process for several depth ranges.

In conclusion, the FDORT method can still be performed to detect point targets in the presence of speckle noise, but the medium needs to be sampled in thin slices to decouple the targets from the speckle noise. The number of significant eigenvalues is the number of targets in the slice, and the eigenvectors are the corresponding Green functions.

IV. THE LOCAL FDORT METHOD

A. Principles

In Sec. III B we proposed gating the signal in depth to reduce coupling. In addition, the volume can be shrunk along the lateral dimension. To perform the method in a zone contained between azimuth $x - \Delta x$ and $x + \Delta x$, only the lines whose azimuth lies between $x - \Delta x$ and $x + \Delta x$ are processed. Thus, using FDORT, we can specify the size of the volume where the method is performed: In azimuth by setting which lines are processed, and in depth by setting the width of the time window. This is shown in Fig. 9.

The lowest lateral extension of the area where one can perform FDORT without losing information about a point scatterer is here about 10 consecutive lines, corresponding to a width of 1.5 mm. This corresponds to the beam width. FDORT performed in such a small window, represented with solid line in Fig. 7, is termed Local FDORT. It processes the signal reflected only from a specific location and gives the first few eigenvalues and eigenvectors. This local algorithm offers the best option to detect a low reflectivity scatterer within speckle; it minimizes the influence of the noise resulting from both coupled speckle (by windowing in depth) and uncoupled speckle (by windowing in azimuth).

A Local DORT method has been performed from a full data set by Kerbrat *et al.*,²³ using a prefocused array. However, they need to repeat the acquisitions for each location where they want to perform DORT and all the transmissions

have to be processed. For the method presented in this paper, only one set of acquisitions is needed, and only 10 transmissions need to be processed for each location. This results in an important savings in processing cost. As it uses focused, and thus localized, transmissions, FDORT is better adapted for local processing than the conventional DORT method.

B. *In vivo* experiments: Application to microcalcification detection

One of the challenges of breast ultrasonic imaging is improved detection of **small microcalcifications**, which can be associated with cancer. Small microcalcifications are often hard to distinguish because of their small size and because they are **embedded in speckle**.

1. Influence of the scatterer nature in the DORT method

When the scatterer size is less than a wavelength, the scatterer is associated with only one nonzero eigenvalue. However, for deterministic scatterers whose size is greater than a wavelength, two or more eigenvalues are observed.¹⁰ Also, for speckle signals, several eigenvalues of similar magnitude are observed, as seen in Fig. 10(a).

A way of detecting small deterministic scatterers like the microcalcifications is to use the **Local FDORT method** and to **consider the ratio of the first two eigenvalues**. If a point scatterer is present at the location, the first eigenvalue is higher than the second one, and the ratio is dramatic. If there is only speckle or an extended reflector, like a cyst edge, the eigenvalues are of similar magnitude and the ratio is close to 1. Considering only the first eigenvalue is not enough, as it is proportional to the echogenicity (reflectivity) which is often greater for extended objects or even speckle; the ratio takes into account the size difference.

2. The moving window FDORT

Local FDORT gives access to the local properties of the medium. Thus it gives the eigenvalues and the ratio of the eigenvalues at a specific location, the **location of the window**. To scan the medium, one needs to move the window at a series of locations. This can be done in depth by **translating the time gate** or in azimuth by **changing the lines processed**. For example, the first window may use lines 1–10, the second window lines 2 to 11, and so on. For each location, the **sizes of the windows are the same**. **Eigenvalues are computed for each position**. This is the moving window FDORT.

3. *In vivo* experiments and results

Experiments are carried out on clinical data. Acquisitions are performed on a healthy female volunteer, using a Philips HDI-5000 scanner with a 1D linear array probe, at 7.3 MHz center frequency. Local FDORT is performed in a window whose dimension is $\Delta z=0.7$ mm and $\Delta x=1$ mm (10 lines). The window is moved along the white line depicted on Fig. 10(b) at a constant depth, where a microcalcification has been identified, using a moving window FDORT. Figure 10(c) shows the variation of the first eigenvalues versus azimuth, at the center frequency. Looking only at the first ei-

genvalue, which is proportional to the reflectivity, we cannot distinguish the microcalcification from the other scatterers. However, when considering the ratio λ_1/λ_2 , in Fig. 10(d), the microcalcification appears clearly. Averaging over several frequencies within the bandwidth improves the results. The process can be repeated for several depths, and a 2D color map can be plotted, but at significant computational cost.

Finally, the eigenvector corresponding to the identified microcalcification has been used in focusing. The resulting field in the medium has been computed and the results are displayed in Fig. 11. This demonstrates the **good focusing property of FDORT's eigenvectors in a clinical application**.

V. CONCLUSION

This paper demonstrates that the DORT method can be successfully generalized to acquisitions with focused transmission beams. It is then termed FDORT. This mode of transmission is the one routinely used by medical ultrasound scanners. If point scatterers are well resolved, each scatterer is associated with an eigenvector given by FDORT, and **focusing on each scatterer can be performed by transmitting the corresponding eigenvector**. DORT and FDORT would be equivalent if each focused pulse was transmitted using the whole aperture of the array (and if enough beams are used to span the region of interest), but this is usually not the case. **The resolution is then lower with FDORT and is limited by the size of the transmit aperture**.

In biological tissue, as in other complex media, **speckle noise dramatically reduce the performance of DORT or FDORT**. We show that this effect is due to speckle located in the zone of coupling (*shadow*) of the scatterers. **The solution is to take advantage of the temporal resolution in an impulsive approach and to sample the medium in slices**. **Gating the signal in depth allows getting rid of most of the noise**, and detection of wires in a tissue-mimicking phantom was performed. Eigenvectors in that case had good focusing properties. **Depth gating takes advantage of the focused transmits of FDORT**, and is not directly compatible with DORT. **Eigenvectors associated with microcalcifications** in clinical data were exhibited, demonstrating the feasibility of the method *in vivo*. Other applications may exist for nondestructive evaluation or detection of objects on ocean floor.

A method to help in microcalcification detection is also proposed. The difference of the FDORT *signature*, **using the ratio of the two first eigenvalues**, between point scatterers, whose size is less than the wavelength, and other scatterers, is exploited. **Using a moving-window algorithm**, a scan highlighting the position of the point scatterers can then be displayed. Again, FDORT is better suited than DORT for this application.

The criterion used to detect the microcalcifications is their size, which is not the most relevant criterion. It has been shown that DORT can also give information on the mechanical properties of the scatterer,¹⁸ and further work should investigate a criterion based on the fact that the material of the microcalcifications is different from the material

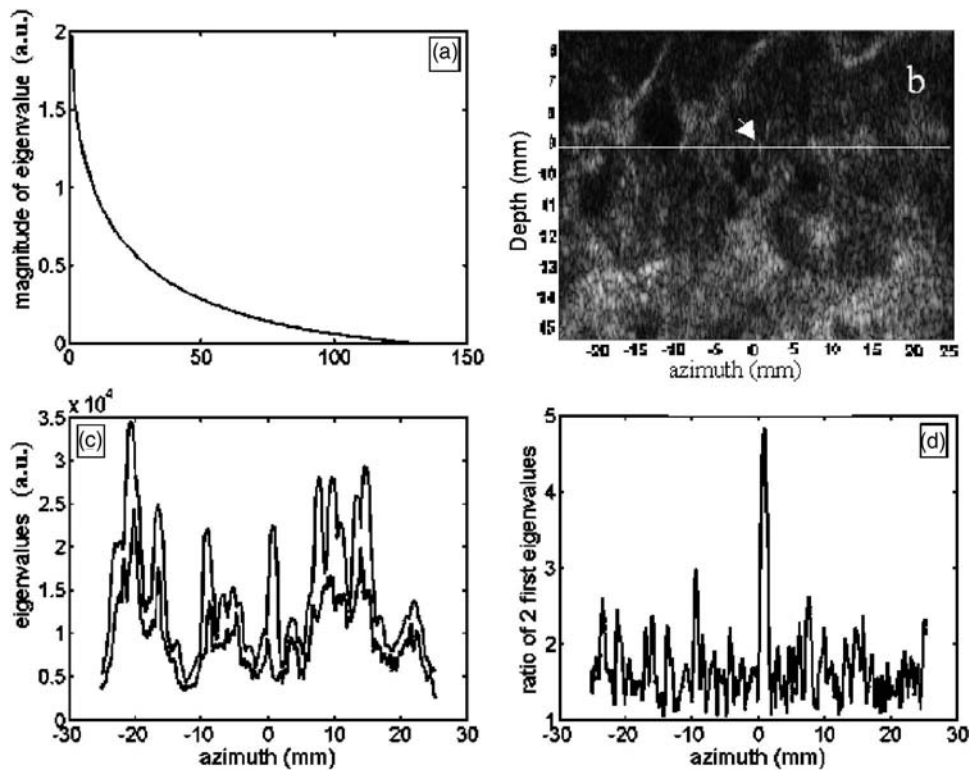


FIG. 10. (a) Eigenvalues in pure speckle in decreasing order: The spectrum is continuous, thus the first two eigenvalues have similar magnitude. FDORT was performed locally in a 0.7 mm deep and 1 mm wide area at several azimuth along the white line depicted on the breast ultrasound image. (b) A scatterer identified as a microcalcification is shown by the white arrow. (c) The first two eigenvalues are plotted vs the azimuth. The first eigenvalue is proportional to the echogenicity, but considering the second eigenvalue adds additional information. (d) Ratio of the first two eigenvalues vs the azimuth: The position of the microcalcification is indicated by a high ratio.

of tissue. It has also been shown that FDORT can focus well even in pure speckle regions.²⁴ This should be investigated and theoretically justified in further studies.

APPENDIX: COUPLING TERM BETWEEN TWO SCATTERERS WITH FDORT

For simplicity, the scatterers are first assumed to be in the focal plane. It is also supposed that all the beam patterns are identical to within a translation, which is usually the case without aberration and not too close to the array edge. Under the Fresnel approximation, the beam patterns in the focal plane are the Fourier transform of the aperture functions. The pattern centered at $x=0$ is given by $F(x) = e^{j\pi x^2/\lambda z} FT[A(X)] \times (x/\lambda z)$, where $A(X)$ is the aperture function and FT is the Fourier transform. We will neglect the complex exponential factor in the following. The beam pattern for a beam centered at azimuth x_i is then $F_i = F(x-x_i)$ and the field sensed by target P is $F_i(P) = F(x_p-x_i)$.

Now the coupling term of Eq. (16) becomes

$$C(Q,P) = \sum_{i=1}^N F_i(Q)F_i(P)^* = \sum_{i=1}^N F(x_Q-x_i)F(x_P-x_i)^*.$$

Using distributions, this can be rewritten as

$$\begin{aligned} C(Q,P) &= \int F(x_Q-x)F(x_P-x)^* \sum_{i=1}^N \delta(x-x_i) dx \\ &= \int F(x) \sum_{i=1}^N \delta(-x-x_i-x_Q) \\ &\quad \times F(x-(x_Q-x_p))^* dx, \end{aligned} \quad (A1)$$

where $\sum_{i=1}^N \delta(-x-x_i-x_Q)$ is a dirac comb multiplied by a gate of width $x_N-x_1=N$ times the beam spacing, and centered on x_Q . The influence of the gate is negligible if N is large enough so that the width of the beam pattern is neglectable compared to N times the beam spacing. The gate will be omitted in the following. The formula (A1) can be interpreted as the cross-correlation between the 2 functions

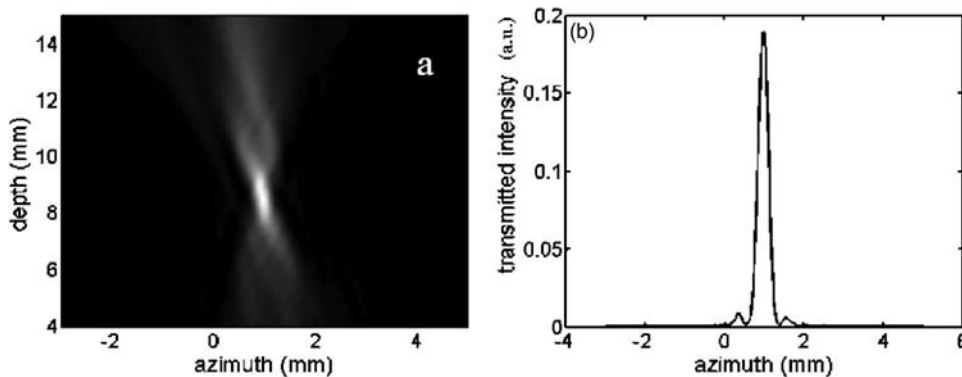


FIG. 11. Focusing achieved in breast clinical data using a microcalcification as a point scatterer. The first eigenvector has been numerically backpropagated. Left: Intensity of the resulting field. Right: Intensity vs azimuth at the depth of the microcalcification.

$F(x)\sum_{i=-\infty}^{+\infty}\delta(-x-x_i-x_Q)$ and $F(x)$ at lag x_Q-x_p . Using Fourier transforms it can be expressed as

$$C(Q,P) = FT \left[FT^{-1} \left(F(x) \sum_{i=-\infty}^{+\infty} \delta(-x-x_i-x_Q) \right) \times FT^{-1}(F(x))^* \right] \left(\frac{x_Q-x_p}{\lambda z} \right). \quad (A2)$$

Now, $FT^{-1}(F(x))=A(X)$ and $FT^{-1}(F(x)\sum_{i=-\infty}^{+\infty}\delta(-x-x_i-x_Q))$ is equal to $A(X)$ convoluted by a Dirac comb. Two Dirac peaks in the comb are separated by $d=\lambda z/\Delta x_i$, where f is the focal length and Δx_i is the beam spacing. If d is greater than the width of the aperture function D , or in other words, if the beam spacing is smaller than the resolution $\lambda z/D$, then Eq. (A2) simplifies to

$$C(Q,P) = C_0 FT[|A(X)|^2] \left(\frac{x_Q-x_p}{\lambda z} \right) = C_0 F(x-\Delta x) \otimes F(-x) = C_0 R_{FF}(\Delta x) = 0. \quad (A3)$$

where C_0 is a constant.

If no apodization is used, $A(X)$ and $|A(X)|^2$ are both the same rectangular windows. Therefore $C(Q,P)=\mathbf{F}(x_Q-x_p)$. The coupling is then weak if the targets' separation is greater than the beam width. In DORT the coupling is proportional to the Fourier transform of the whole array; in FDORT it depends on the aperture function used for each transmission.

If there are aberrations at the transducer surface, the aperture function becomes $A(X)e^{i\phi(X)}$. As only the modulus of the aperture function is considered in the coupling term, it is not affected by the aberration as long as only a phase shift is introduced.

If the targets are out of the focal plane, the field in the plane of the targets can be expressed by the Fourier transform of $A(X)e^{i\phi(X)}$ with $\phi(X)=(\pi/\lambda z)X^2$. The phase term also disappears when the modulus is taken. The coupling should then not depend on the focal length.

¹M. O'Donnell and S. W. Flax, "Phase-aberration correction using signals from point reflectors and diffuse scatterers: Measurements," IEEE Trans. Ultrason. Ferroelectr. Freq. Control **35**, 768–774 (1998).

²R. C. Gauss, M. S. Soo, and G. E. Trahey, "Wavefront distortion measurements in the human breast," IEEE Ultrasonic Symposium Proceedings, 1547–1551 (1997).

³R. C. Gauss, G. E. Trahey, and M. S. Soo, "Wavefront estimation in the human breast" Proc. SPIE **4325**, 172–181 (2001).

⁴D. L. Liu, J. A. Baker, and P. Von Behren, "A clinical study of adaptive beamforming using time-delay adjustments on a 1D array," IEEE Ultra-

sonic Symposium Proceedings, **1**, 339–342 (2003).

⁵J. J. Dahl and G. E. Trahey, "Off-axis scatterer filters for improved aberration measurements," IEEE Ultrasonic Symposium Proceedings, 343–347 (2003).

⁶M. Fink, "Time reversal of ultrasonic fields-Part I: Basic principles," IEEE Trans. Sonics Ultrason. **39**(5), 555–566 (1992).

⁷C. Prada, F. Wu, and M. Fink, "The iterative time reversal mirror: A solution to self-focusing in the pulse echo mode," J. Acoust. Soc. Am. **90**(2), 1119–1129 (1991).

⁸C. Prada and M. Fink, "Eigenmodes of the time reversal operator: A solution to selective focusing in multiple-target media," Wave Motion **20**, 151–163 (1994).

⁹C. Prada, S. Manneville, D. Spoliansky, and M. Fink, "Decomposition of the time reversal operator: Application to detection and selective focusing on two scatterers" J. Acoust. Soc. Am. **99**, 2067–2076 (1996).

¹⁰S. Komilikis, C. Prada, and M. Fink, "Characterization of extended objects with the DORT method," IEEE Ultrasonic Symposium Proceedings, 1401–1404 (1996).

¹¹A. J. Devaney, "Computational time reversal and object localization," J. Acoust. Soc. Am. **110**, 2617 (2001); A. J. Devaney, "Super-resolution processing using time reversal and music," J. Acoust. Soc. Am. (unpublished).

¹²A. B. Baggeroer, W. A. Kupperman, and P. N. Mikhalevsky, "An overview of matched field methods in ocean acoustics," IEEE J. Ocean. Eng. **18**(4), (1993).

¹³C. Prada and J.-L. Thomas, "Experimental subwavelength localization of scatterers by decomposition of the time reversal operator interpreted as a covariance matrix," J. Acoust. Soc. Am. **113**(6), 1–9 (2003).

¹⁴J. G. Berryman *et al.*, "Statistically stable ultrasonic imaging in random media," J. Acoust. Soc. Am. **112**, 1509–1522 (2002).

¹⁵T. D. Mast, A. L. Nachman, and R. C. Waag, "Focusing and imaging using eigenfunctions of the scattering operator," J. Acoust. Soc. Am. **102**, 715–725 (1997).

¹⁶C. F. Gaumond, D. M. Fromm, J. Lingeitch, R. Menis, G. Edelmann, D. Calvo, and E. Kim "Application of DORT to active sonar," MTS/IEEE TECHNO-OCEAN **4**, 2230–2235 (2004).

¹⁷C. Prada, M. Tanter, and M. Fink, "Flaw detection in solid with the DORT method" IEEE Ultrasonic Symposium Proceedings, 681–686 (1997).

¹⁸D. H. Chambers and A. K. Gautesen, "Time reversal for a spherical scatterer," J. Acoust. Soc. Am. **109**, 2616–2624 (2001).

¹⁹C. H. Frazier and W. D. O'Brien, "Synthetic aperture technique with a virtual source element," IEEE Trans. Ultrason. Ferroelectr. Freq. Control **45**(1), 196–207 (1998).

²⁰K. L. Gammelmark and J. A. Jensen, "Multielement synthetic transmit aperture imaging using temporal encoding," IEEE Trans. Med. Imaging **22**(4), 552–563 (2003).

²¹M. Fink and J. Cardoso, "Diffraction effects in pulse-echo measurements," IEEE Trans. Sonics Ultrason. **31**, 313–329 (1984).

²²R. Mallart and M. Fink, "Adaptative focusing in scattering media through sound speed inhomogeneities: The Van Cittert Zernike approach and focusing criterion," J. Acoust. Soc. Am. **96**(6), 3721–3732 (1994).

²³E. Kerbrat, C. Prada, D. Cassereau, and M. Fink, "Imaging in the presence of grain noise using the decomposition of the time reversal operator," J. Acoust. Soc. Am. **113**, 1230–1240 (2003).

²⁴Michael R. Burcher, Anna. T. Fernandez, and Claude Cohen-bacrie, "A novel phase aberration technique derived from the D.O.R.T. method: Comparison with correlation based method on simulated and *in vivo* data," IEEE Ultrasonic Symposium Proceedings, August 2004.

Copyright of *Journal of the Acoustical Society of America* is the property of American Institute of Physics and its content may not be copied or emailed to multiple sites or posted to a listserv without the copyright holder's express written permission. However, users may print, download, or email articles for individual use.